

# Mathematical Modeling of the Single-Phase Multicomponent Flow in Porous Media <sup>\*</sup>

Petr Gális<sup>1</sup>[0000–0003–3176–6458] and Jiří Mikyška<sup>1</sup>[0000–0001–6017–2259]

Department of mathematics, Faculty of Nuclear Sciences and Physical Engineering,  
Czech Technical University in Prague, Czech Republic, [galispet@fjfi.cvut.cz](mailto:galispet@fjfi.cvut.cz)

**Abstract.** A numerical scheme of higher-order approximation in space for the single-phase multicomponent flow in porous media is presented. The mathematical model consists of Darcy velocity, transport equations for components of a mixture, pressure equation and associated relations for physical quantities such as viscosity or density. The discrete problem is obtained via discontinuous Galerkin method for the discretization of transport equations with the combination of mixed-hybrid finite element method for the discretization of Darcy velocity and pressure equation both using higher-order approximation. Subsequent problem is solved with the fully mass-conservative iterative IMPEC method. Numerical experiments of 2D flow are carried out.

**Keywords:** Compositional flow · Mixed-hybrid finite element method · Discontinuous Galerkin method.

## 1 Introduction

The compositional modeling has many applications in various disciplines ranging from petroleum engineering (oil recovery, CO<sub>2</sub> sequestration) to geochemical engineering (groundwater contamination, radioactive waste storage in the subsurface). Modeling of such phenomena is therefore of a great importance. In this work we consider the single-phase flow of miscible and compressible multicomponent fluids in porous media. We follow an approach of the previous works of [6], [7], [12], [13] based on the combination of the mixed-hybrid finite element (MHFEM) for the approximation of the pressure and velocity fields and discontinuous Galerkin method (DG) for the approximation of transport equations. Hoteit and Firoozabadi [7] and Moortgat, Sun and Firoozabadi [13] used a combination of MHFEM for the pressure equation and higher-order DG method for the transport equations. Although they used piecewise linear basis functions for

---

<sup>\*</sup> The work was supported by the Czech Science Foundation project no. 21-09093S Multiphase flow, transport, and structural changes related to water freezing and thawing in the subsurface, by the Ministry of Education, Youth and Sports of the Czech Republic under the OP RDE grant number CZ.02.1.01/0.0/0.0/16\_019/0000778 Centre for Advanced Applied Sciences, and by the Student Grant Agency of the Czech Technical University in Prague, grant no. SGS20/184/OHK4/3T/14.

the concentrations, they used only piecewise constant functions for the pressures and  $\mathbb{RT}_0$  (i.e. first-order) approximation for the velocity field. They also used a different form of the pressure equation which seems to be more complicated than the one used in [8]. In contrast to classical IMPEC schemes, used in the previous works and which are known to have a mass-conservation problem, Chen, Fan and Sun [8] have rewritten the pressure equation with only one additional parameter to be determined and proposed a new fully mass-conservative IMPEC scheme where conservation of mass for all components holds true. So far only the first-order approximation for pressure and velocity field has been utilized in the models. In this work we show how to extend these ideas for the higher-order framework. In contrast to previous works we apply higher order scheme not only for the transport of the species but also for the pressure and the velocity fields.

## 2 Mathematical model

Consider single-phase compressible flow of fluid of  $n_c$  components at constant temperature  $T$  [K] in a bounded domain  $\Omega \subset \mathbb{R}^2$  with porosity  $\phi$  [-]. In this work we assume that the porosity does not depend on time, i.e. we have  $\phi = \phi(\mathbf{x})$ . Neglecting diffusion, the transport of the components is described by the following equations

$$\frac{\partial(\phi c_i)}{\partial t} + \nabla \cdot (c_i \mathbf{v}) = f_i, \quad i = 1, \dots, n_c, \quad (1)$$

where  $c_i$  [mol · m<sup>-3</sup>] are molar concentrations of components,  $f_i$  [mol · m<sup>-3</sup> · s<sup>-1</sup>] are source/sink terms and  $\mathbf{v}$  [m · s<sup>-1</sup>] is the velocity field described by the Darcy's law

$$\mathbf{v} = -\mu^{-1} \mathbf{K} (\nabla p - \rho \mathbf{g}), \quad (2)$$

where  $p$  [Pa], is the pressure field,  $\mu$  [kg · m<sup>-1</sup> · s<sup>-1</sup>] is the dynamic viscosity,  $\rho$  [kg · m<sup>-3</sup>] is the density of fluid,  $\mathbf{K}$  [m<sup>2</sup>] is the medium permeability tensor and  $\mathbf{g}$  [m · s<sup>-2</sup>] is the gravity acceleration vector. Equations (1) and (2) are coupled with generally nonlinear dependencies

$$p = p(c_1, \dots, c_{n_c}, T), \quad \mu = \mu(c_1, \dots, c_{n_c}, T), \quad \rho = \rho(c_1, \dots, c_{n_c}). \quad (3)$$

to be found in [11] or [15]. Using the chain rule  $\frac{\partial p}{\partial t} = \sum_{i=1}^{n_c} \frac{\partial p}{\partial c_i} \frac{\partial c_i}{\partial t}$  and transport equations (1), we derive an equation for the pressure field

$$\phi \frac{\partial p}{\partial t} + \sum_{i=1}^{n_c} \theta_i [\nabla \cdot (c_i \mathbf{v}) - f_i] = 0, \quad (4)$$

where parameters  $\theta_i = \theta_i(c_1, \dots, c_{n_c})$  are defined as  $\theta_i = \left(\frac{\partial p}{\partial c_i}\right)_{c_j \neq c_i}$  as in [8]. Let  $I \subset \mathbb{R}$  be a time interval. The initial and boundary conditions are given by

$$\begin{aligned} c_i(0, \mathbf{x}) &= c_i^0(\mathbf{x}), & \mathbf{x} \in \Omega, \quad i = 1, \dots, n_c, \\ c_i(t, \mathbf{x}) &= c_i^D(\mathbf{x}), & \mathbf{x} \in \Gamma_c, \quad t \in I, \quad i = 1, \dots, n_c, \\ p(t, \mathbf{x}) &= p^D(t, \mathbf{x}), & \mathbf{x} \in \Gamma_p, \quad t \in I, \\ \mathbf{v}(t, \mathbf{x}) \cdot \mathbf{n}(\mathbf{x}) &= v^N(t, \mathbf{x}), & \mathbf{x} \in \Gamma_v, \quad t \in I, \end{aligned} \quad (5)$$

where  $\mathbf{n}$  is the outward unit normal vector to the boundary  $\partial\Omega$ ,  $\Gamma_p \cup \Gamma_v = \partial\Omega$  and  $\Gamma_p \cap \Gamma_v = \emptyset$ . Note that the initial pressure field is obtained from the equation of state (3) by substituting  $c_i^0$ ,  $i = 1, \dots, n_c$ . Further, we define the inflow part of boundary  $\Gamma_c(t) = \{\mathbf{x} \in \partial\Omega \mid \mathbf{v}(t, \mathbf{x}) \cdot \mathbf{n}(\mathbf{x}) < 0\}$  on which Dirichlet-type conditions  $c_i^D$  must be prescribed. On  $\Gamma_c \cap \Gamma_p$  the following constraint must be satisfied  $p^D = p(c_1^D, \dots, c_{n_c}^D, T)$ . The source terms  $f_i$  in (1) and (4) are usually expressed via injection rate  $r$  [ $\text{m}^3 \cdot \text{s}^{-1}$ ] as  $f_i = c_i^{inj} r / V^{inj}$  where  $c_i^{inj}$  is the amount of  $i$ -th component injected in some part of the domain with the volume  $V^{inj}$ . Similarly, Neumann boundary condition  $v^N$  in (5) is often expressed as  $v^N = r / A^{inj}$  where  $A^{inj}$  is the area through which the mixture is injected.

### 3 Numerical model

A discrete form of the system of equations (1) - (3) and (4), (5) is obtained using the mixed-hybrid finite element method for the Darcy's law and the pressure equation and discontinuous Galerkin method for the transport equations. We consider a polygonal domain  $\Omega \subset \mathbb{R}^2$  covered with a conforming triangulation  $\mathcal{T}_h$ . Let us denote by  $\mathcal{E}_h$  the set of all edges in the triangulation  $\mathcal{T}_h$ . For the  $K \in \mathcal{T}_h$  and  $E \in \mathcal{E}_h$  we denote  $|K|$  and  $|E|$  the measures of the element  $K$  and edge  $E$ , respectively. The triangulation consists of  $n_k$  triangle elements and  $n_e$  edges.

#### 3.1 Discretization of Darcy's law

The velocity field is approximated in the Raviart-Thomas space  $\mathbb{RT}_1(K)$  locally on the element  $K \in \mathcal{T}_h$  as

$$\mathbf{v}_K(t, \mathbf{x}) = \sum_{j=1}^8 v_{K,j}(t) \mathbf{w}_{K,j}(\mathbf{x}), \quad (6)$$

where  $\mathbb{RT}_1(K) = \text{span}\{\mathbf{w}_{K,j}\}_{j=1}^8$  and  $v_{K,j}$  are associated degrees of freedom. The definition of the  $\mathbb{RT}_1(K)$  space is taken over from [3]. The basis  $\{\hat{\mathbf{w}}_j\}_{j=1}^8$  on the reference element  $\hat{K}$  (see Figure 1) is obtained via the following moments

$$\begin{aligned} N_s^\alpha(\hat{\mathbf{w}}_j) &= \int_{e_\alpha} (\hat{\mathbf{w}}_j \cdot \mathbf{n}_\alpha) p_s, & \forall p_s \in \mathbb{P}_1(e_\alpha), \quad s = 1, 2, \quad \alpha = 1, 2, 3, \\ M_r(\hat{\mathbf{w}}_j) &= \int_{\hat{K}} (\hat{\mathbf{w}}_j \cdot \mathbf{q}_r), & \forall \mathbf{q}_r \in [\mathbb{P}_0(\hat{K})]^2, \quad r = 1, 2, \end{aligned}$$

where  $\mathbb{P}_1(e_\alpha) = \text{span}\{p_s\}_{s=1}^2$  is the space of linear polynomials defined on the edge  $e_\alpha$  of the reference element and  $[\mathbb{P}_0(\hat{K})]^2 = \text{span}\{\mathbf{q}_r\}_{r=1}^2$  is the space of vector-valued constant polynomials. The discrete form of Darcy's law is obtained by multiplying (2) by a basis function  $\mathbf{w}_{K,m}$ , integrating over the element  $K$  and using Green's theorem

$$v_{K,m} = \mu_K^{-1} \left( \sum_{j=1}^3 \sum_{l=1}^8 [\alpha_{m,l}^K \beta_{l,j}^K] p_{K,j} - \sum_{E \in \partial K} \sum_{s=1}^2 \sum_{l=1}^8 [\alpha_{m,l}^K \chi_{l,s}^{K,E}] \hat{p}_{E,s} + \rho_K \sum_{l=1}^8 \alpha_{m,l}^K \gamma_l^K \right), \quad m = 1, \dots, 8, \quad (7)$$

where  $\mu_K, \rho_K$  denote the mean values of viscosity and density over the element  $K$ , respectively. In the derivation of (7) we used the following approximation of the pressure and pressure trace on the element  $K$  and edge  $E$

$$p(t, \mathbf{x})|_K = \sum_{j=1}^3 p_{K,j}(t) \Phi_{K,j}(\mathbf{x}), \quad p(t, \mathbf{x})|_E = \sum_{s=1}^2 \hat{p}_{E,s}(t) \varphi_s^E(\mathbf{x}), \quad (8)$$

where  $\mathbb{P}_1(K) = \text{span}\{\Phi_{K,j}\}_{j=1}^3$  and  $\mathbb{P}_1(E) = \text{span}\{\varphi_j^E\}_{j=1}^2$  are spaces of linear polynomials defined on the element  $K$  and on the edge  $E$ , respectively. The coefficients in (7) are given by

$$\begin{aligned} \tilde{\alpha}_{m,j}^K &= \int_K \mathbf{w}_{K,m} \cdot \mathbf{K}^{-1} \mathbf{w}_{K,j}, & \beta_{m,j}^K &= \int_K \Phi_{K,j} (\nabla \cdot \mathbf{w}_{K,m}), \\ \chi_{m,s}^{K,E} &= \int_E \varphi_s^E (\mathbf{w}_{K,m} \cdot \mathbf{n}_E^K), & \gamma_m^K &= \int_K \mathbf{g} \cdot \mathbf{w}_{K,m}, \end{aligned} \quad (9)$$

where the coefficients  $\alpha_{i,j}^K$  are elements of the inverse matrix  $(\tilde{\alpha}^K)^{-1}$ . In order to compute integrals in (9) on the reference element we use the following affine transformation of variables  $F_K : \hat{K} \rightarrow K$  and the transformation of the vector-valued function which preserves normal components

$$\begin{aligned} F_K(s, t) &= \begin{pmatrix} x_1 \\ y_1 \end{pmatrix} + J_{F_K} \begin{pmatrix} s \\ t \end{pmatrix}, & J_{F_K} &= \begin{pmatrix} x_2 - x_1 & x_3 - x_1 \\ y_2 - y_1 & y_3 - y_1 \end{pmatrix}, \\ \mathbf{w}_{K,m}(x, y) &= \frac{1}{|J_{F_K}|} J_{F_K} \cdot \hat{\mathbf{w}}_m(s, t), & (s, t) &= F_K^{-1}(x, y) \in \hat{K}, \end{aligned} \quad (10)$$

where  $(x_i, y_i)$ ,  $i = 1, 2, 3$  are the coordinates of vertices of the physical element  $K$  and  $|J_{F_K}|$  is the determinant of the matrix  $J_{F_K}$ . Continuity of the normal component of the velocity field along the edges shared by neighboring elements is enforced through the conditions [2]

$$\sum_{K \in \mathcal{T}_h} \langle \mathbf{v} \cdot \mathbf{n}^K, \varphi_1^E \rangle_{\partial K} = 0, \quad \sum_{K \in \mathcal{T}_h} \langle \mathbf{v} \cdot \mathbf{n}^K, \varphi_2^E \rangle_{\partial K} = 0 \quad \forall E \in \mathcal{E}_h, \quad (11)$$

where  $\langle f, g \rangle_{\partial K} = \int_{\partial K} fg$ . Denoting by  $\sum_{K \in E}$  the sum over adjacent elements to the given edge  $E$ , continuity conditions (11) can be further simplified to

$$\sum_{K \in E} v_{K, LI(K, E, s)} \chi_{LI(K, E, s), s}^{K, E} = 0, \quad s = 1, 2, \quad \forall E \in \mathcal{E}_h, \quad (12)$$

where  $LI(K, E, s) \in \{1, 2, 3, 4, 5, 6\}$  is the local index of the velocity degree of freedom for  $s \in \{1, 2\}$  on the edge  $E$  with respect to the element  $K$ , see Figure 1. As the degrees of freedom  $v_{K,7}$  and  $v_{K,8}$  are associated with basis functions  $\mathbf{w}_{K,7}$  and  $\mathbf{w}_{K,8}$ , which have zero normal component along the boundary  $\partial K$  of the element  $K$ , these do not play any role when enforcing the continuity constraint. The discrete form of the boundary and initial conditions (5) reads as

$$\begin{aligned} \hat{p}_{E,s} &= p_s^D|_E, \quad s = 1, 2, \quad \forall E \subset \Gamma_p, \\ v_{K, LI(K, E, s)} &= v_s^N|_E, \quad s = 1, 2, \quad \forall E \subset \Gamma_v, \quad E \in \partial K. \end{aligned} \quad (13)$$

The velocity can be eliminated substituting (7) into (12) and (13) resulting in the system of linear algebraic equations for pressures  $p$  and pressure traces  $\hat{p}$

$$\begin{aligned} & \sum_{K \in E} \sum_{m=1}^3 \sum_{l=1}^8 \left[ \mu_K^{-1} \chi_{r,j}^{K,E} \alpha_{r,l}^K \beta_{l,m} \right] p_{K,m} - \sum_{s=1}^2 \sum_{K \in E} \sum_{F \in \partial K} \sum_{l=1}^8 \left[ \mu_K^{-1} \chi_{r,j}^{K,E} \alpha_{r,l}^K \chi_{l,s}^{K,F} \right] \hat{p}_{F,s} \\ &= v_j^N|_{(E \cap \Gamma_v)} - \sum_{K \in E} \mu_K^{-1} \rho_K \chi_{r,j}^{K,E} \sum_{l=1}^8 \alpha_{r,l}^K \gamma_l^K, \quad j = 1, 2, \quad \forall E \not\subset \Gamma_p, \\ \hat{p}_{E,j} &= p_j^D|_E, \quad j = 1, 2, \quad \forall E \subset \Gamma_p, \end{aligned} \quad (14)$$

where  $r = LI(K, E, j)$ .

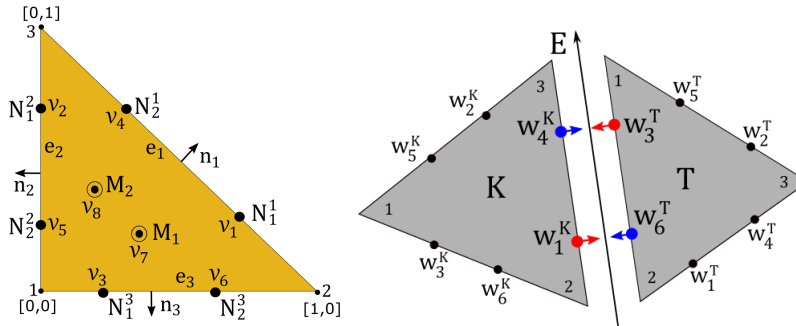


**Fig. 1.** Reference element and degrees of freedom (left). Local indexing of the neighboring triangles sharing an edge (right). For this setup values of indexing function are  $LI(K, E, 1) = 1$ ,  $LI(K, E, 2) = 4$ ,  $LI(T, E, 1) = 3$ ,  $LI(T, E, 2) = 6$ .

### 3.2 Discretization of pressure and transport equations

In the discontinuous Galerkin discretization we use linear approximation of the concentrations in the space  $\mathbb{P}_1(K)$

$$c_i(t, \mathbf{x})|_K = \sum_{j=1}^3 c_{K,i,j}(t) \Phi_{K,j}(\mathbf{x}). \quad (15)$$

We recall that we assume  $\phi = \phi(\mathbf{x})$ . Multiplying (1) by the basis function  $\Phi_{K,m} \in \mathbb{P}_1(K)$ , integrating over the element  $K$  and using Green's theorem, we derive a discrete form of (1) for  $i = 1, \dots, n_c$  and  $m = 1, 2, 3$

$$\frac{dc_{K,i,m}}{dt} = \frac{1}{\phi_K} \sum_{q=1}^3 \eta_{m,q}^K \left( F_{i,q}^K - \sum_{j=1}^8 v_{K,j} \left[ \sum_{E \in \partial K} \delta_{i,q,j}^{K,E} - \sum_{l=1}^3 \tau_{q,j,l}^K c_{K,i,l} \right] \right), \quad (16)$$

where the following definitions were used

$$\begin{aligned} \tilde{\eta}_{m,j}^K &= \int_K \Phi_{K,m} \Phi_{K,j}, & \delta_{i,m,j}^{K,E} &= \int_E \hat{c}_{K,i,E} (\mathbf{w}_{K,j} \cdot \mathbf{n}_E^K) \Phi_{K,m}, \\ F_{i,m}^K &= \int_K f_i \Phi_{K,m}, & \tau_{m,j,l}^K &= \int_K \Phi_{K,l} (\mathbf{w}_{K,j} \cdot \nabla \Phi_{K,m}). \end{aligned} \quad (17)$$

The coefficients  $\tilde{\eta}_{i,j}^K$  are elements of the inverse matrix  $(\tilde{\eta}^K)^{-1}$ . Note that coefficients  $\delta$  and  $F$  are time dependent. In (17) the quantity  $\hat{c}_{K,i,E}$  is the upwinded value of the concentration  $c_i$  on the edge  $E$  with respect to the element  $K$  and velocity  $\mathbf{v}$ .

A discrete version of the pressure equation (4) is derived in a similar manner as the discrete transport equation with additional substitution of (7) into  $v_{K,j}$

$$\frac{dp_{K,m}}{dt} = \sum_{f=1}^3 \sigma_{m,f}^K p_{K,f} + \sum_{s=1}^2 \sum_{E \in \partial K} \lambda_{m,s}^{K,E} \hat{p}_{E,s} + \Gamma_m^K + \Sigma_m^K, \quad m = 1, 2, 3, \quad (18)$$

where we used

$$\begin{aligned} \sigma_{m,f}^K &= \frac{-1}{\phi_K \mu_K} \sum_{q=1}^3 \eta_{m,q}^K \sum_{j=1}^8 \sum_{l=1}^8 \alpha_{l,j}^K \beta_{j,f}^K \sum_{i=1}^{n_c} \theta_{K,i} \omega_{K,i,q,j}, \\ \lambda_{m,s}^{K,E} &= \frac{1}{\phi_K \mu_K} \sum_{q=1}^3 \eta_{m,q}^K \sum_{j=1}^8 \sum_{l=1}^8 \alpha_{l,j}^K \chi_{l,s}^{K,E} \sum_{i=1}^{n_c} \theta_{K,i} \omega_{K,i,q,j}, \\ \Gamma_m^K &= \frac{-\rho_K}{\phi_K \mu_K} \sum_{q=1}^3 \eta_{m,q}^K \sum_{j=1}^8 \sum_{l=1}^8 \alpha_{l,j}^K \gamma_l^K \sum_{i=1}^{n_c} \theta_{K,i} \omega_{K,i,q,j}, \\ \Sigma_m^K &= \frac{1}{\phi_K} \sum_{q=1}^3 \eta_{m,q}^K \sum_{i=1}^{n_c} \theta_{K,i} F_{i,q}^K, \quad \omega_{K,i,q,j} = \sum_{F \in \partial K} \delta_{i,q,j}^{K,F} - \sum_{r=1}^3 \tau_{q,j,r}^K c_{K,i,r} \end{aligned} \quad (19)$$

and by  $\theta_{K,i}$  we denoted the mean value of the coefficient  $\theta_i$  over the element  $K$ .

### 3.3 Iterative IMPEC

For the solution of the given non-linear problem we use the fully mass-conservative iterative IMPEC method proposed in [8]. We made the following change in the algorithm. In this work the pressure is initialized using the EOS from the given concentrations  $p^n = p(c_{i=1, \dots, n_c}^n)$  as opposed to [8], where the pressure  $p^n$  is taken as the solution pressure from the previous time step. This way, the error from the discretization will not cumulate as the simulation goes on. Given a solution  $(c_1^n, \dots, c_{n_c}^n)$  at the  $n$ -th time level, to obtain pressure field and concentrations at the  $(n+1)$ -th time level we proceed iteratively as follows.

1. Set  $l = 0$  and  $p^{n+1,0} = p^n = p(c_1^n, \dots, c_{n_c}^n)$ ,  $c_i^{n+1,0} = c_i^n$ , for  $i = 1, \dots, n_c$ . The boundary values are evaluated at the  $(n+1)$ -th time level. Values of  $\theta_i^{n+1}$  are initially estimated using the EOS as  $\theta_i^{n+1,0} = \frac{\partial p}{\partial c_i}(c_1^n, \dots, c_{n_c}^n)$ .
2. Repeat
  - (a) Set  $l = l + 1$ .
  - (b) The following problem is solved with the MHFEM for pressures  $p^{n+1,l}$ , pressure traces  $\hat{p}^{n+1,l}$  and velocity  $\mathbf{v}^{n+1,l}$  (for details see below)

$$\begin{aligned} \phi \frac{p^{n+1,l} - p^n}{\Delta t} + \sum_{i=1}^{n_c} \theta_i^{n+1,l-1} \left[ \nabla \cdot \left( c_i^{n+1,l-1} \mathbf{v}^{n+1,l} \right) - f_i^{n+1} \right] &= 0, \\ \mathbf{v}^{n+1,l} &= -\frac{1}{\mu^{n+1,l-1}} \mathbf{K} \left[ \nabla p^{n+1,l} - \rho^{n+1,l-1} \mathbf{g} \right], \end{aligned} \quad (20)$$

- (c) Values of  $c_i^{n+1,l}$  for  $i = 1, \dots, n_c$  are explicitly updated as (for details see below)

$$\phi \frac{c_i^{n+1,l} - c_i^n}{\Delta t} + \nabla \cdot \left( c_i^{n+1,l-1} \mathbf{v}^{n+1,l} \right) = f_i^{n+1}. \quad (21)$$

- (d) A slope limiter for  $c_i^{n+1,l}$ ,  $i = 1, \dots, n_c$ , is applied.
- (e) Parameters  $\theta_i^{n+1,l}$  are updated using the difference formula

$$\theta_i^{n+1,l} = \frac{p(\xi_i) - p(\eta_i)}{c_i^{n+1,l} - c_i^n}, \quad (22)$$

where

$$\begin{aligned} \xi_i &= (c_1^{n+1,l}, \dots, c_{i-1}^{n+1,l}, c_i^{n+1,l}, c_{i+1}^n, \dots, c_{n_c}^n), \\ \eta_i &= (c_1^{n+1,l}, \dots, c_{i-1}^{n+1,l}, c_i^n, c_{i+1}^n, \dots, c_{n_c}^n). \end{aligned}$$

Computation of  $p(\cdot)$  in the nominator (22) is based on the EOS.

(f) Iteration stops when  $\max\{E_p, E_c, E_\theta\} < \delta$  where

$$\begin{aligned} E_p &= \frac{\|p^{n+1,l} - p^{n+1,l-1}\|_{L_2(\Omega)}^2}{\|p^{n+1,l}\|_{L_2(\Omega)}^2}, \\ E_c &= \sum_{i=1}^{n_c} \frac{\|c_i^{n+1,l} - c_i^{n+1,l-1}\|_{L_2(\Omega)}^2}{\|c_i^{n+1,l}\|_{L_2(\Omega)}^2}, \\ E_\theta &= \sum_{i=1}^{n_c} \frac{\|\theta_i^{n+1,l} - \theta_i^{n+1,l-1}\|_{L_2(\Omega)}^2}{\|\theta_i^{n+1,l}\|_{L_2(\Omega)}^2}. \end{aligned} \quad (23)$$

If the criterion is met we then set  $p^{n+1} = p^{n+1,l}$ ,  $\mathbf{v}^{n+1} = \mathbf{v}^{n+1,l}$  and  $c_i^{n+1} = c_i^{n+1,l}$  for  $i = 1, \dots, n_c$ . Otherwise we go back to step (a).

We now describe the step 2 of the algorithm in more details. In (b), as the pressures  $p^{n+1,l}$  can be eliminated, the system is solved for pressure traces  $\hat{p}^{n+1,l}$  only by means of the equations (14) and (18) with the time discretization as in (20). The underlying system of linear equations for pressure traces  $\hat{p}^{n+1,l}$  have the followig form

$$\begin{aligned} p^{n+1,l} + \mathbf{D}^{-1}\mathbf{H}_1 \hat{p}_1^{n+1,l} + \mathbf{D}^{-1}\mathbf{H}_2 \hat{p}_2^{n+1,l} &= \mathbf{D}^{-1}\mathbf{G}, \\ \mathbf{R}_1 p^{n+1,l} - \mathbf{M}_{1,1} \hat{p}_1^{n+1,l} - \mathbf{M}_{1,2} \hat{p}_2^{n+1,l} &= \mathbf{V}_1, \\ \mathbf{R}_2 p^{n+1,l} - \mathbf{M}_{2,1} \hat{p}_1^{n+1,l} - \mathbf{M}_{2,2} \hat{p}_2^{n+1,l} &= \mathbf{V}_2, \end{aligned} \quad (24)$$

from which the elimination of the pressures is apparent. The matrices in (24) can be deduced from (14) and (18), see e.g. [6]. The velocity field  $\mathbf{v}^{n+1,l}$  is then computed according to (6) by evaluating (7). The mean values of  $\mu^{n+1,l-1}$  and  $\rho^{n+1,l-1}$  are computed at  $(c_1^{n+1,l-1}, \dots, c_{n_c}^{n+1,l-1})$ . In (c), the semi-discrete equation (16) is used with the time discretization as in (21). Such time discretization leads to an explicit scheme for  $c_{K,i}^{n+1,l}$ , because only  $c_{K,i}^{n+1,l-1}$  are present. Upwind values  $\hat{c}_{K,i,E}^{n+1,l-1}$  in (20) and (21) are evaluated as follows

$$\hat{c}_{K,i,E}^{n+1,l-1}(\mathbf{x}) = \begin{cases} c_{K,i}^{n+1,l-1}(\mathbf{x}), & \mathbf{v}_K^{n+1,l-1} \cdot \mathbf{n}_E^K(\mathbf{x}) \geq 0, & \mathbf{x} \in E \\ c_{T,i}^{n+1,l-1}(\mathbf{x}), & \mathbf{v}_K^{n+1,l-1} \cdot \mathbf{n}_E^K(\mathbf{x}) < 0, & \mathbf{x} \in E \notin \partial\Omega, \\ c_i^{D,n+1}(\mathbf{x}), & \mathbf{v}_K^{n+1,l-1} \cdot \mathbf{n}_E^K(\mathbf{x}) < 0, & \mathbf{x} \in E \subset \Gamma_c. \end{cases} \quad (25)$$

Note that concentrations  $c_{K,i}^{n+1,l-1}$  or  $c_{T,i}^{n+1,l-1}$  are computed using (15) on the elements  $K$  or  $T$ , respectively. Evaluation of the difference formula in (e) is discussed in the section 4.4. For slope limiting procedure in (d), we refer the reader to [9]. We note that the choice of the slope limiter greatly affects the convergence behavior of the iterative IMPEC algorithm.

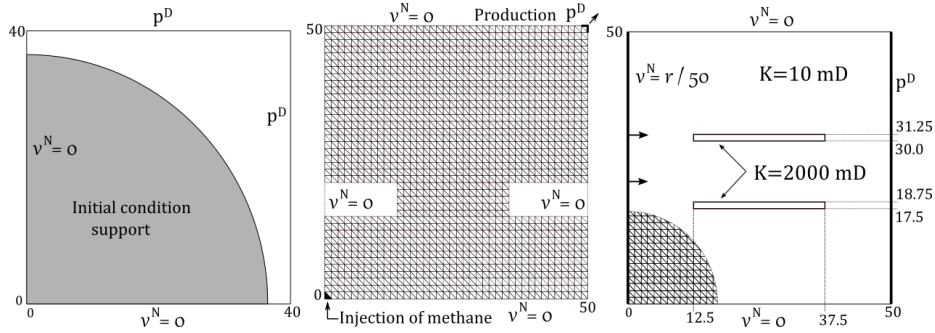


**Fig. 2.** Structure of the computational meshes for Example 1 (left), Example 2 (middle) and Example 3 (right).

## 4 Numerical examples

### 4.1 Example 1

Example 1 serves to verify higher-order approximation of the numerical scheme with the use of experimental order of convergence (EOC) analysis. Let us consider the following problem

$$\frac{\partial c}{\partial t} + \nabla \cdot (c\mathbf{v}) = 0, \quad \mathbf{v} = -2\nabla p, \quad (26)$$

with the equation of state of the form  $p(c) = c$  and initial and boundary condition

$$\begin{aligned} c(t_0, \mathbf{x}) &= B_2(t_0, \mathbf{x}), \quad \mathbf{x} \in \Omega, \\ p(t, \mathbf{x}) &= B_2(t, \mathbf{x}), \quad \mathbf{x} \in \Gamma_p, \quad t \in (t_0, t_1), \\ \mathbf{v}(t, \mathbf{x}) \cdot \mathbf{n}(\mathbf{x}) &= 0, \quad \mathbf{x} \in \Gamma_v, \quad t \in (t_0, t_1), \end{aligned} \quad (27)$$

where  $\Omega = [0, 40] \times [0, 40] \text{ m}^2$ ,  $t_0 = 7500\text{s}$ ,  $t_1 = 45000\text{s}$ . Function  $B_m = B_m(t, \mathbf{x})$  is the well-known Barenblatt solution given by

$$B_m(t, \mathbf{x}) = \max \left\{ 0, t^{-\alpha} \left( \Lambda - \frac{\alpha(m-1)}{2dm} \frac{|\mathbf{x}|^2}{t^{2\alpha/d}} \right)^{\frac{1}{m-1}} \right\}. \quad (28)$$

In (28) we choose  $d = 2$ ,  $m = 2$ ,  $\alpha = (m-1 + 2/d)^{-1} = 1/2$  and  $\Lambda = 1$ . We further define the Dirichlet and Neumann boundaries as

$$\begin{aligned} \Gamma_p &= \{ (x, 40) \cup (40, y) \mid x \in (0, 40), y \in (0, 40) \}, \\ \Gamma_v &= \{ (0, y) \cup (x, 0) \mid y \in (0, 40), x \in (0, 40) \}. \end{aligned} \quad (29)$$

The EOC and errors are included in the Table 1. The computational mesh is parametrized with a parameter  $h \in \mathbb{N}$  as  $n_k = 2 \times 4h \times 4h$  (structured triangular mesh). We choose  $\Delta t \sim h^{-2}$  so that the error from the time discretization does not interfere with the space discretization. The error is computed by interpolating (28) into the basis of  $\mathbb{P}_1(K)$  for each  $K \in \mathcal{T}_h$ . Tolerance for the stopping criterion (23) is chosen as  $\delta = 1.49 \times 10^{-12}$ .

**Table 1.** Experimental order of convergence and errors at time  $t_1$  for Example 1.

h	$\Delta t$	$\ E_h\ _{L_1}$ $EOC_1$	$\ E_h\ _{L_2}$ $EOC_2$	$\ E_h\ _{L_\infty}$ $EOC_\infty$
4	18.75	$5.2228 \times 10^{-3}$	$1.3792 \times 10^{-4}$	$3.6610 \times 10^{-6}$
8	4.6875	$1.1837 \times 10^{-3}$ 2.1415	$3.1263 \times 10^{-5}$ 2.1413	$8.6644 \times 10^{-7}$ 2.0791
16	1.1719	$2.9109 \times 10^{-4}$ 2.0238	$7.6769 \times 10^{-6}$ 2.0258	$2.1072 \times 10^{-7}$ 2.0398
32	$2.9297 \times 10^{-1}$	$7.3970 \times 10^{-5}$ 1.9764	$1.9481 \times 10^{-6}$ 1.9785	$5.1956 \times 10^{-8}$ 2.0199
64	$7.3242 \times 10^{-2}$	$1.7480 \times 10^{-5}$ 2.0812	$4.6140 \times 10^{-7}$ 2.0780	$1.2901 \times 10^{-8}$ 2.0099
128	$1.8311 \times 10^{-2}$	$5.2721 \times 10^{-6}$ 1.7293	$1.3844 \times 10^{-7}$ 1.7368	$3.2146 \times 10^{-9}$ 2.0047

## 4.2 Example 2

In Example 2, we will try to reproduce numerical results in [15]. Let us consider a reservoir  $\Omega = [0, 50] \times [0, 50] \text{ m}^2$  with porosity  $\phi = 0.2$  and permeability  $\mathbf{K} = 10^{-14} \mathbf{I} \text{ m}^2$  at initial pressure  $p = 5 \times 10^6 \text{ Pa}$  and temperature  $T = 397 \text{ K}$  in a horizontal position with  $\mathbf{g} = (0, 0) \text{ m/s}^2$  or vertical position with  $\mathbf{g} = (0, -9.81) \text{ m/s}^2$  initially filled with propane. In the corner  $\{(x, y) \mid 0 \leq x \leq 1.25, 0 \leq y \leq 1.25 - x\}$  pure methane with concentration (molar density)  $c^{inj} = 42.2896 \text{ mol/m}^3$  is injected with the injection rate  $r = 3.90625 \times 10^{-4} \text{ m}^3/\text{s}$ . Mixture of propane and methane is produced on the boundary  $\{(x, 50) \mid 48.75 \leq x \leq 50\} \cup \{(50, y) \mid 48.75 \leq y \leq 50\}$  where pressure  $p = 5 \times 10^6 \text{ Pa}$  is maintained. The rest of the boundary is impermeable, i.e. zero Neumann condition  $v^N = 0$  is imposed. Relevant data for the Peng-Robinson EOS are taken over from [15] and listed in Table 2. The binary interaction coefficient of the methane-propane is  $k_{12} = 0.0365$ . The mesh consists of  $2 \times 40 \times 40$  triangular elements. The time step is chosen constant  $\Delta t = 6000 \text{ s}$  for both horizontal and vertical case. Tolerance for the stopping criterion (23) is chosen as  $\delta = 1.49 \times 10^{-7}$ .

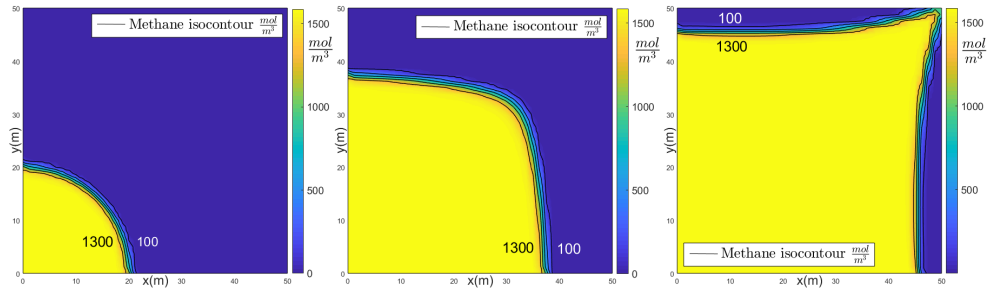


**Fig. 3.** Contours of methane from Example 2 with  $\mathbf{g} = (0, 0)$  at the time  $t = 6 \times 10^6 \text{ s}$  (left),  $t = 24 \times 10^6 \text{ s}$  (middle) and  $t = 48 \times 10^6 \text{ s}$  (right).

## 4.3 Example 3

In Example 3, we will try to reproduce numerical results of the Example 6.5 in [8]. Let us consider a reservoir  $\Omega = [0, 50] \times [0, 50] \text{ m}^2$  with porosity  $\phi = 0.2$  and

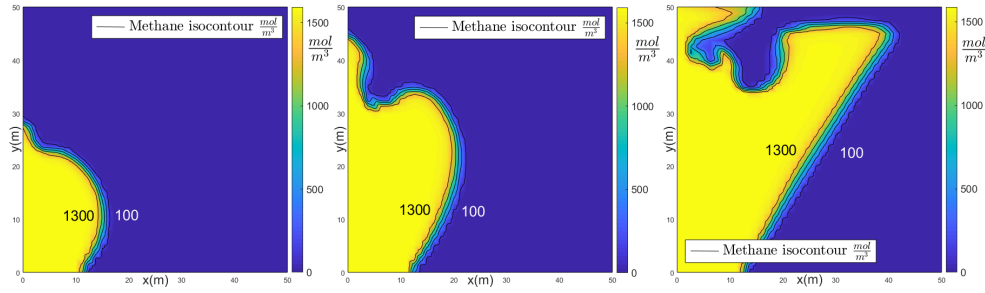


**Fig. 4.** Contours of methane from Example 2 with  $\mathbf{g} = (0, -9.81)$  at the time  $t = 6 \times 10^6 s$  (left),  $t = 12 \times 10^6 s$  (middle) and  $t = 21.6 \times 10^6 s$  (right).

**Table 2.** Peng-Robinson EOS parameters for the Example 2.

component	$p_{ci}$ [Pa]	$T_{ci}$ [K]	$V_{ci}$ [ $\text{m}^3 \text{mol}^{-1}$ ]	$M_i$ [ $\text{kg mol}^{-1}$ ]	$\omega_i$ [-]
1 (methane)	$4.58373 \cdot 10^6$	$1.89743 \cdot 10^2$	$9.897054 \cdot 10^{-5}$	$1.62077 \cdot 10^{-2}$	$1.14272 \cdot 10^{-2}$
2 (propane)	$4.248 \cdot 10^6$	$3.6983 \cdot 10^2$	$2.000001 \cdot 10^{-4}$	$4.40962 \cdot 10^{-2}$	$1.53 \cdot 10^{-1}$

permeability distribution

$$\mathbf{K} = \begin{cases} 2000 \text{ mD} \times \mathbf{I}, & \{(x, y) | x \in (12.5, 37.5), y \in (17.5, 18.75) \cup (30, 31.25)\} \\ 10 \text{ mD} \times \mathbf{I}, & \text{elsewhere,} \end{cases}$$

at initial pressure  $p = 1.5 \times 10^5$  Pa and temperature  $T = 554.8$  K initially filled with propane. On the whole west boundary  $\{(0, y) | 0 \leq y \leq 50\}$  the mixture of methane and ethane with total concentration (molar density)  $c^{inj} = 32.527 \text{ mol/m}^3$  is injected with the injection rate  $r = 3.17 \times 10^{-6} \text{ m}^3/\text{s}$ . Molar fractions of the injecting mixture are 0.8 for methane and 0.2 for the ethane. The mixture is produced on the whole east boundary  $\{(50, y) | 0 \leq y \leq 50\}$  where pressure  $p = 1.5 \times 10^5$  Pa is maintained. The rest of the boundary is impermeable, i.e. zero Neumann condition  $v^N = 0$  is imposed. Relevant data for the Peng-Robinson EOS are taken over from [5] and listed in Table 3. The binary interaction coefficients are  $k_{12} = -0.0026$  for the methane-ethane,  $k_{13} = 0.014$  for the methane-propane and  $k_{23} = 0.011$  for the ethane-propane. For the viscosity, the Lee-Gonzalez model [10] is selected. The mesh and the convergence criterion is the same as for Example 2.

#### 4.4 Update of $\theta$ parameter

When computing parameters  $\theta_i$ , we have to deal with special case  $c_i^{n+1, l} \rightarrow c_i^n$  for which the denominator in (22) approaches zero. In [8] this is treated in the following perturbation manner. If  $|c_i^{n+1, l}| < \varepsilon$  and  $|c_i^{n+1, l} - c_i^n| < \varepsilon$ , that is  $c_i^{n+1, l}$  and  $c_i^n$  are both close to zero, we then set  $c_i^{n+1, l} := c_i^n + \varepsilon$ . Else if

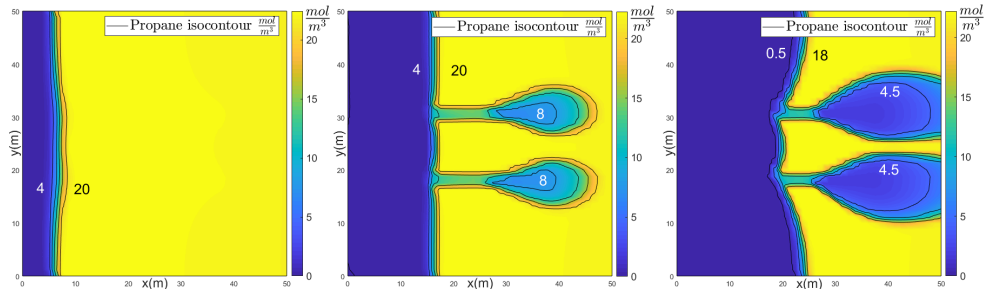


**Fig. 5.** Contours of propane from Example 3 at the time  $t = 17.4 \times 10^6 s$  (left),  $t = 52.2 \times 10^6 s$  (middle) and  $t = 86.4 \times 10^6 s$  (right).

**Table 3.** Peng-Robinson EOS parameters for the Example 3.

component	$p_{ci}$ [Pa]	$T_{ci}$ [K]	$V_{ci}$ [ $\text{m}^3 \text{kg}^{-1}$ ]	$M_i$ [ $\text{kg mol}^{-1}$ ]	$\omega_i$ [-]
1 (methane)	$4.604 \cdot 10^6$	$1.9058 \cdot 10^2$	$6.17284 \cdot 10^{-3}$	$1.62077 \cdot 10^{-2}$	$0.04348 \cdot 10^{-1}$
2 (ethane)	$4.880 \cdot 10^6$	$3.0542 \cdot 10^2$	$4.92611 \cdot 10^{-3}$	$3.070 \cdot 10^{-2}$	$1.0109 \cdot 10^{-1}$
3 (propane)	$4.250 \cdot 10^6$	$3.6982 \cdot 10^2$	$4.608295 \cdot 10^{-3}$	$4.40962 \cdot 10^{-2}$	$1.5788 \cdot 10^{-1}$

$|c_i^{n+1,l} - c_i^n| < \varepsilon |c_i^{n+1,l}|$ , that is  $c_i^{n+1,l}$  and  $c_i^n$  are close to each other, we set  $c_i^{n+1,l} := c_i^n + \varepsilon c_i^{n+1,l}$ . These perturbations are used for the parameter update step only. When all the updates are done, the values of  $c_i^{n+1,l}$  are reset to their original values. The  $\varepsilon$  value is chosen as the square root of machine precision. In this paper, we try to pursue this problem with the use of

$$\lim_{c_i^n \rightarrow c_i^{n+1,l}} \theta_i^{n+1,l} = \left( \frac{\partial p}{\partial c_i} \right) (c_1^{n+1,l}, \dots, c_{i-1}^{n+1,l}, c_i^{n+1,l}, c_{i+1}^n, \dots, c_{n_c}^n). \quad (30)$$

In Figure 6 we compare both approaches by plotting the numbers of iterations which are needed to converge at each time level in the step 2 of the iterative IMPEC algorithm in Example 2. The tolerance for the stopping criterion (23) is chosen as  $\delta = 1.49 \times 10^{-7}$ . From the given comparison we concluded, that the formula (30) can be utilized as well as the perturbation treatment given in [8]. If we choose stronger tolerance for the stopping criterion (e.g.  $\delta = 1.49 \times 10^{-8}$ ), then the iterative IMPEC algorithm would have trouble satisfying stopping criterion for  $E_\theta$  as can be seen in Figure 7. The problem is that even though concentrations converge with respect to the stopping criterion, the error  $E_\theta$  does not further decrease.

## 5 Conclusions

In this work we have shown how to extend modeling of the multicomponent compressible single-phase Darcy flow in porous media based on the combination

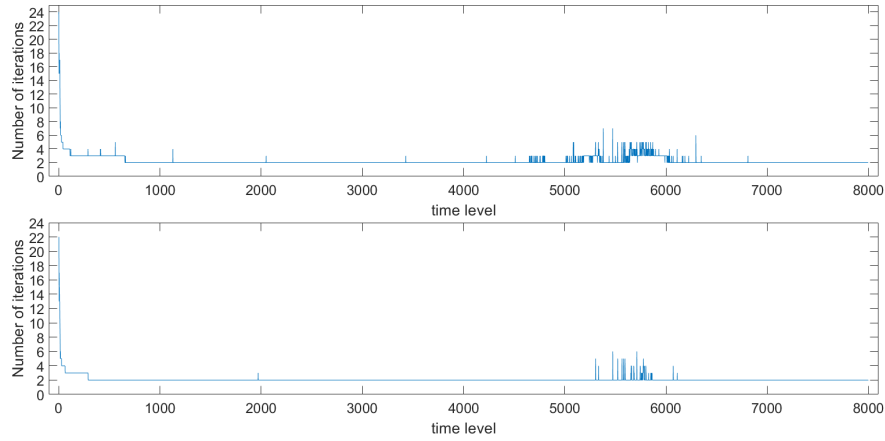


**Fig. 6.** Number of iteration needed to converge at each time level using perturbation (top) and limit (30) (bottom) approaches. Tolerance  $\delta = 1.49 \times 10^{-7}$  is chosen.

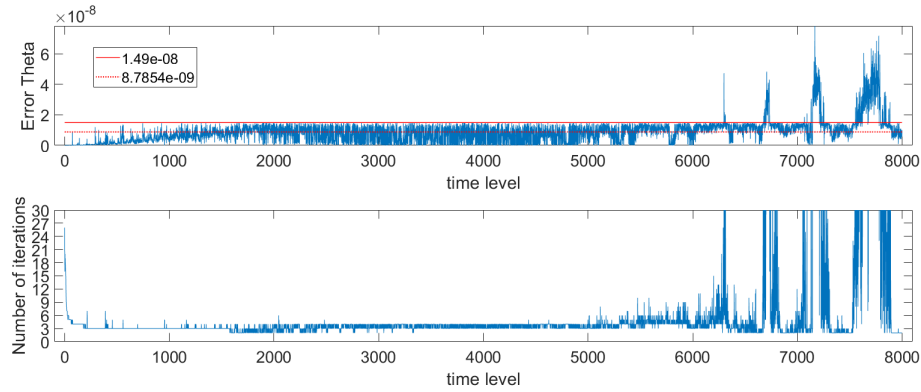


**Fig. 7.** Error  $E_\theta$  (top) and number of iteration needed to converge (bottom) at each time level for the tolerance  $\delta = 1.49 \times 10^{-8}$ . In the later stage of the simulation the convergence criterion is not satisfied for many time steps as the  $E_\theta$  does not decrease.

of MHFEM and DG methods to a higher-order approximation scheme. The main extension is the use of the higher-order Raviart-Thomas space for the approximation of the velocity field. The system of nonlinear algebraic equations for concentration, pressure and velocity fields obtained by combining the MHFEM and DG is solved with the fully mass-conservative iterative IMPEC scheme in which the given equation of state is incorporated through the pressure equation with an additional nonlinear parameter. Three numerical experiments were performed. The first example gave a proof of the expected second order approximation in space through the computation of EOC. The second and the third examples were taken over from the literature to verify the correctness of the code. In the second example the outcome was positive and we obtained the

same results. In the third example we obtained different results from the original authors. We believe that such outcome is only a consequence of different interpretation of the source terms. In the experiments, the proposed derivative approach was used in the update of the pressure equation parameters which slightly improved the convergence of the method. In the future work, we would like to improve the current model with the inclusion of a diffusive term in the transport equations and with the higher-order time discretization.

## References

1. Ács G., Doleschall S., Farkas É.: General purpose compositional model. *Society of Petroleum Engineers Journal*, vol. 25, 543–553 (1985)
2. Brezzi F., Douglas J., Fortin M., Marini L. D.: Efficient Rectangular Mixed Finite Elements in Two and Three Space Variables. *Modélisation mathématique et Analyse numérique*, vol. 21, 581–604 (1987)
3. Brezzi F., Fortin M.: Mixed and Hybrid Finite Element Methods. *Springer Series in Computational Mathematics*, vol. 15 (1991)
4. Boffi D., F. Brezzi, M. Fortin.: Mixed Finite Element Methods and Applications. *Springer Series in Computational Mathematics*, vol. 44, Springer Science & Business Media, (2013)
5. Firoozabadi A.: *Thermodynamics of Hydrocarbon Reservoirs*. McGraw-Hill Education (1999)
6. Hoteit H., Firoozabadi A.: Multicomponent Fluid Flow by Discontinuous Galerkin and Mixed Methods in Unfractured and Fractured Media, *Water Resources Research* (2005). <https://doi.org/10.1029/2005WR004339>.
7. Hoteit H., Firoozabadi A.: Compositional Modeling By the Combined Discontinuous Galerkin and Mixed Methods, *Society of Petroleum Engineers* (2006)
8. Chen H., Fan X., Sun S.: A Fully Mass-Conservative Iterative IMPEC Method for Multicomponent Compressible Flow in Porous Media. *Journal of Computational and Applied Mathematics*, vol. 362, 1–21 (2019)
9. Barth T., Jespersen D.: The design and application of upwind schemes on unstructured meshes, *27th Aerospace Sciences Meeting* (1989)
10. Lee A. L., Gonzalez M. H., Eakin B. E.: The Viscosity of Natural Gases. *Journal of Petroleum Technology*, vol. 18, 997–1000 (1966)
11. Lohrenz J., Bray B. G., Clark C. R.: Calculating Viscosities of Reservoir Fluids From Their Compositions. *Journal of Petroleum Technology*, vol. 16, 1171–1176 (1964)
12. Moortgat J., Firoozabadi A.: Mixed-hybrid and Vertex-Discontinuous-Galerkin Finite Element Modeling of Multiphase Compositional Flow on 3D Unstructured Grids. *Journal Computational Physics*, vol. 315, 476–500 (2016)
13. Moortgat J., Sun S., Firoozabadi A.: Compositional Modeling of Three-Phase Flow With Gravity Using Higher-Order Finite Element Methods. *Water Resources Research*, vol. 47 (2011). <https://doi.org/10.1029/2010WR009801>.
14. Polívka O., Mikyška J.: Combined Mixed-Hybrid Finite Element–Finite Volume Scheme for Computation of Multicomponent Compressible Flow in Porous Media. *Numerical Mathematics and Advanced Applications*, Springer-Verlag, 559–567 (2011)
15. Polívka O., Mikyška J.: Numerical Simulation of Multicomponent Compressible Flow in Porous Medium. *Journal of Math for Industry*, vol. 3, 53–60 (2013)